Multitemporal analysis of PAL images for the study of land cover dynamics in South America

J.A. Sobrino [a,*], Y. Julien [a], L. Morales [b,c]

[a] *Global Change Unit, Department of Thermodynamics, University of Valencia, c/ Dr Moliner, 50, 46100, Burjassot, Spain*
[b] *Departamento de Física, Universidad Tecnológica Metropolitana, Av. José Pedro Alessandri 1242, Casilla 9845, Santiago, Chile*
[c] *Departamento de Ciencias Ambientales y Recursos Naturales Renovables, Facultad de Ciencias Agronómicas, Universidad de Chile, A. Santa Rosa 11315, Casilla 1004, Santiago, Chile*

Abstract

Pathfinder AVHHR Land (PAL) database has been used for the retrieval of Land Surface Temperature (LST) over South America, which, along with NDVI parameter, will allow the studying of the evolution of the vegetation between July 1981 and September 2001. To this end, a classification has been built, based on PAL NDVI and Reanalysis air temperature at 2 m height data. This classification takes into account both vegetation and thermal patterns, and has been validated by a comparison with CAZALAC's map of arid zones (Centro del Agua para Zonas Áridas y semiáridas de Latino-América y el Caribe), as well as with Global Land Cover Characteristics' classification built by the USGS (United States Geological Survey). The principal advantage of this new classification is that it is a dynamic classification, that considers the actual state of the cover, since no assumption on land occupation is made for its construction. LST and NDVI yearly and long-term evolutions are analyzed with the help of this classification. Yearly evolutions are compared with Reanalysis air temperature at 2 m height and precipitation, and show good concordance. LST long-term evolution shows to be strongly affected by satellite changes and orbital drift. These latter require an adequate correction to allow deeper study. On the other hand, NDVI does not show this trend, but aerosol absorption from Mount Pinatubo's eruption in June 1991 corrupts temporarily the data. These results also validate the above-mentioned classification.

Keywords: land surface temperature; NDVI; classification; PAL

1. Introduction

Pathfinder AVHRR Land (PAL) is up to now the largest database of satellite images available. It provides global images of the Earth at an 8·8 km spatial resolution, and at a 10-day temporal resolution, from July 1981 until September 2001. For each 10-day time-period are available four composite images, at visible (red — Ch1), near infrared (Ch2) and thermal infrared (Ch4 and Ch5) wavelengths, as well as an image of NDVI. The compositing technique consists in selecting for each pixel the day for which the NDVI value is maximum, chosen within a period of 10 consecutive days. The characteristics of this database make it a powerful tool to evaluate changes in vegetation over the past years, due to human factors (deforestation, changes in cultivated areas) as well as climatic change.

* Corresponding author. Tel./fax: +34 96 354 31 15.
E-mail address: sobrino@uv.es (J.A. Sobrino).

From the five images a day provided, several methods (Ulivieri et al., 1994; Sobrino and Raissouni, 2000) have been developed to estimate such parameter as Land Surface Temperature. In this paper, the latest method will be applied, which will allow, with NDVI data, the study of the vegetation. In this work, we will concentrate the study on the South American area.

To achieve this goal, some data from the meteorological database Reanalysis will also be used, such as air temperature at 2 m and precipitation. This database has been elaborated by the NCEP (National Center for Environmental Prediction) and the NCAR (National Center for Atmospheric Research), and contains different meteorological data at a 2.5° resolution, from 1948, and is actualized every month. Data are available with a temporal resolution from 6 h to one month (Kistler et al., 2001).

To this end will first be exposed the algorithm used to determine LST, through emissivity and total atmospheric water vapor estimation, then the classification used to describe the study area will be presented. Finally the preliminary results obtained with this classification will be exposed.

2. Algorithms

In order to calculate Land Surface Temperature the method developed by Sobrino and Raissouni (2000) will be used. First, emissivity will be estimated (from NDVI values) and then total atmospheric water vapor. Because PAL data come without cloud filtering at continental scale, a cloud detection algorithm was developed and is shown further on.

2.1. NDVI

These data are provided directly in PAL database, since they are used to elaborate the 10-day composite images. The NDVI is calculated using the reflectance at red (Ch1) and near-infrared (Ch2) wavelengths:

$$\mathrm{NDVI} = \frac{(\mathrm{Ch2} - \mathrm{Ch1})}{(\mathrm{Ch2} + \mathrm{Ch1})} \tag{1}$$

2.2. Emissivity

Following Sobrino and Raissouni (2000), the image has been divided into three zones, according to their NDVI values. The mean emissivity ε (average of the emissivities for channels 4 and 5 of the AVHRR) and the spectral variation of emissivity $\Delta\varepsilon$ (emissivity difference between both channels) are estimated as follows (all equations are taken from Sobrino and Raissouni, 2000):

NDVI < 0.2:
The surface is assumed to be bare soil, which emissivity is calculated from channel 1 reflectance:

$$\varepsilon = 0.980 - 0.042 \cdot \mathrm{Ch1} \tag{2}$$

$$\Delta\varepsilon = -0.003 - 0.029 \cdot \mathrm{Ch1} \tag{3}$$

0.2 < NDVI < 0.5:
The surface is assumed to be a mix of bare soil and vegetation, which emissivity can be estimated from the proportion of vegetation P_v:

$$\varepsilon = 0.971 + 0.018 \cdot P_v \tag{4}$$

$$\Delta\varepsilon = 0.006 \cdot (1 - P_v) \tag{5}$$

where P_v is calculated from the NDVI itself :

$$P_v = (\mathrm{NDVI} - 0.2)^2 / 0.09 \tag{6}$$

NDVI > 0.5:
The surface is assumed to be vegetation only, so the emissivity can be estimated as:

$$\varepsilon = 0.985 \tag{7}$$

$$\Delta\varepsilon = 0 \tag{8}$$

This method allows emissivity estimation with an error of 0.01 (Sobrino et al., 1999).

2.3. Total atmospheric water vapor

The total atmospheric water vapor is estimated using the variance–covariance ratio (R_{54}), which is calculated from a neighborhood of N pixels of channels 4 and 5 images:

$$R_{54} = \frac{\sum_{k=1}^{N} (T_{4k} - T_{4o})(T_{5k} - T_{5o})}{\sum_{k=1}^{N} (T_{4k} - T_{4o})^2} \tag{9}$$

where T_{4k} and T_{5k} are respectively the radiometric temperatures for each pixel of the neighborhood in channels 4 and 5 images, and T_{4o} and T_{5o} are respectively the average values for the neighborhood in channels 4 and 5 images. From this ratio the total atmospheric water vapor (W) is estimated, according to:

$$W = 0.26 - 14.253\cos(\theta)\ln R_{54} - 11.649(\cos(\theta)\ln R_{54})^2 \tag{10}$$

This method gives an estimation of total atmospheric water vapor with an error of 0.5 $g \cdot cm^{-2}$ (Sobrino et al., 1999).

2.4. Land surface temperature

From the values estimated above (average emissivity, spectral variation of emissivity and water vapor), Land Surface Temperature (T_s) is obtained using the following formula:

$$T_s = T_4 + 1.40 \cdot (T_4 - T_5) + 0.32 \cdot (T_4 - T_5)^2 + 0.83 + (57 - 5W) \cdot (1 - \varepsilon) - (161 - 30W) \cdot \Delta\varepsilon \quad (11)$$

This temperature is obtained with an error of 1.3 K (Sobrino and Raissouni, 2000).

2.5. Cloud detection

The procedure to detect and screening clouds in the PAL dataset is derived from the method developed by Saunders and Kriebel (1988). Since PAL dataset does not include night images, the five tests described in the method were reduced to the following three:

$$\text{Ch1} > A \text{ and } T_s < 280 \text{ K} \quad (12)$$

$$Q = \frac{\text{Ch2}}{\text{Ch1}} < 1.6 \text{ and } T_s < 280 \text{ K} \quad (13)$$

$$\Delta T = (T_4 - T_5) > B(T_4) \quad (14)$$

where A is a dynamic threshold established as three times the reflectance value (for the channel 1) corresponding to the average of land values, and where $B(T_4)$ is a threshold value function of radiometric temperature T_4, which values can be found in Saunders and Kriebel (1988), along with more details about this method. If any of those three tests is true, then the pixel is considered as cloud contaminated.

3. Classification

Since the database is composed of 713 images of 801×601 pixels, a pixel-by-pixel study would be time-consuming, so the authors decided to use a classification of the study area. To allow change detection in vegetation patterns, the classification should be based only on the data. But because of the problem of orbital drift dependence of the thermal data acquired by AVHRR sensor (Price, 1991), a classification method based only on the 20-year NDVI and Land Surface Temperature data, such as the one described in Nemani and Running (1997), is not possible. So Reanalysis Air Temperature at 2 m height was chosen to palliate LST data for the building of the classification, these Reanalysis data being a good indicator of thermal variations.

To this aim, the classification detailed in this study is built from two different classifications, the first one identifying the vegetation type of the area, the second one its thermal pattern. This thermal classification is needed since different types of vegetation can have similar first and second statistic moments while their temporal evolution is quite different. For example, the maximum of NDVI for vegetation in arid areas happens one to three months sooner than in temperate areas. If thermal pattern is ignored, these two different vegetation types could be mixed in the same class, which would not show a coherent evolution in time, being an average of these two behaviors. Moreover, this kind of classification does not use any information a priori, such as land occupation, which would prevent the observation of changes in the studied areas.

3.1. Vegetation classification

This parallelepiped classification is constructed using the method described in Morales et al. (2004), which consists in calculating an average year of NDVI values. This is done first by averaging all the images acquired during January of each year, as to obtain an average image of January, and then repeating this procedure with all the months of the year. From this average year, the mean value and the variation coefficient of the NDVI are computed. The variation coefficient (C_V) is calculated as:

$$C_V = 100 \times \frac{\sigma}{\overline{n}} \quad (15)$$

where $\overline{n}$ is the average value of NDVI, and σ is the standard deviation of NDVI during the average year. This coefficient is a measure of variability of NDVI during the year, which can be analyzed as seasonality of the vegetation. Once these two values for each pixel of the study zone obtained, nine classes are distinguished, depending of the value of both parameters. NDVI values are separated as follow:

NDVI $\leq$ 0.2: bare soil,
0.2 < NDVI $\leq$ 0.5: mix of bare soil and vegetation,
NDVI > 0.5: vegetation only,

while variation coefficient values are separated using:

$C_V \leq 3\%$: low variability,
$3\% < C_V \leq 6\%$: medium variability,
$C_V > 6\%$: high variability.

The classification obtained is shown Fig. 1. In this classification can be differentiated low average NDVI values (classes 1 to 3) from medium NDVI values (classes 4 to 6) and from high NDVI values (classes 7 to 9). The lower variation coefficient values correspond to classes 1, 4 (almost non existent) and 9. Then, medium variation coefficient values correspond to classes 2, 5 and 8, while higher values correspond to classes 3, 6 and 7. Classes 1 and 2 can be identified as mountain areas, while class 3 is composed of arid and semiarid areas. Classes 4, 5 and 6 can be identified as pasture and cultivated land. Class 7 is a mixture of cultivated areas and of forests, while classes 8 and 9 are composed of tropical rainforest.

3.2. Thermal patterns classification

This second classification is not built from PAL data, but from the air temperature at 2 m height, obtained from Reanalysis by the University of Delaware (USA). This data is used to calculate, for an average year, the degree-days (Dg), as introduced by Réaumur (1735). The Dg are obtained from all the days of an average year, selecting the ones which mean Air Temperature (T) is above 10 °C, according to:

$$\mathrm{Dg} = \sum (T - 10\ ^{\circ}\mathrm{C}) \tag{16}$$

This way, a map of the study area is obtained, which can be divided in five zones, according to the thermal pattern defined by Thornthwaite (1948):

$\mathrm{Dg} < 500$: microthermal,
$500 \leq \mathrm{Dg} < 1000$: infrathermal,
$1000 \leq \mathrm{Dg} < 3000$: mesothermal,
$3000 \leq \mathrm{Dg} < 5000$: suprathermal,
$\mathrm{Dg} > 5000$: macrothermal.

The classification obtained is shown Fig. 2. In this classification can be identified the classes 1 and 2 as the coldest ones, corresponding to mountain and austral

Fig. 1. Vegetation classification. The lower classes represent poor vegetation areas, while higher classes represent dense vegetation.

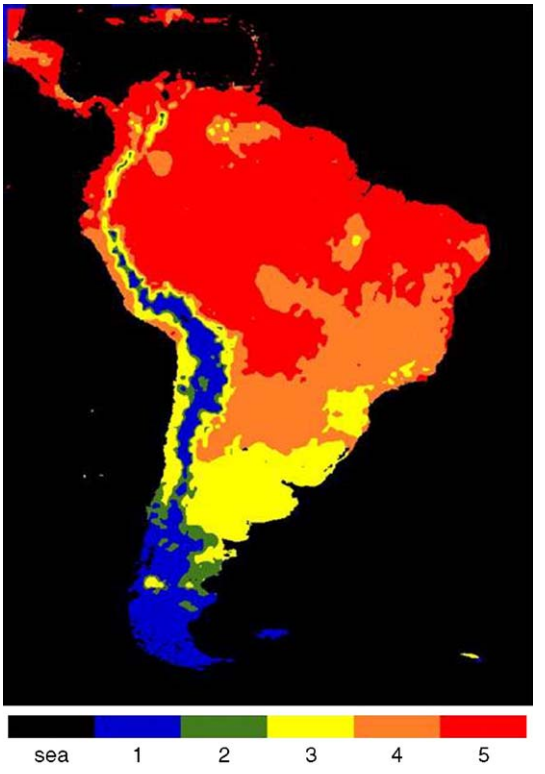

Fig. 2. Thermal pattern classification. The thermal patterns are the following: 1 — microthermal; 2 — infrathermal; 3 — mesothermal; 4 — suprathermal; 5 — macrothermal.

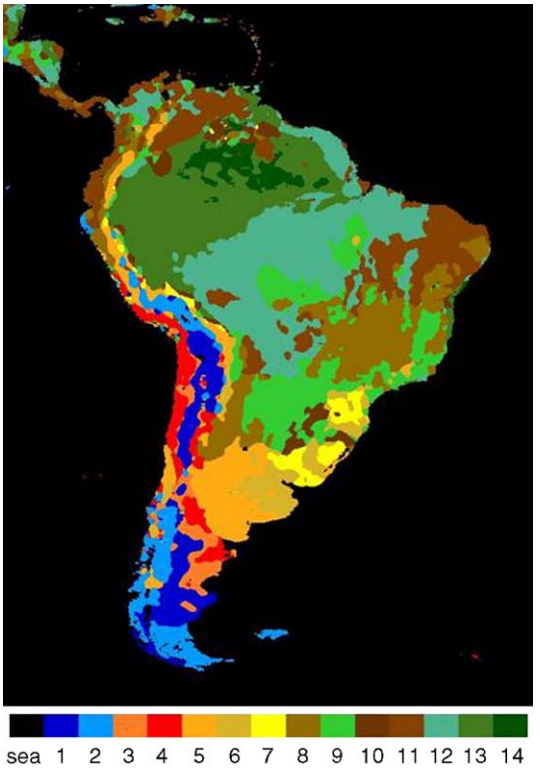

Fig. 3. Final classification. The first 3 classes are associated with mountain areas, class number 4 concerns arid and semi-arid areas, while classes 11 to 14 concern tropical forests.

areas. Then, class 3 corresponds to the most arid areas, while classes 4 and 5 consist mainly of rainforest and cultivated land.

3.3. Final classification

From the nine classes obtained from the first classification, and from the five classes retrieved from the second one, the final classification is elaborated. Out of the 45 possible classes are obtained 41 classes, but some of them with a very low number of pixels, so all classes with less than one thousand pixels are redistributed to the geographically closest classes. Once realized this operation, a majority filter is passed on the image, which leaves 14 different classes. The first 3 classes are associated with mountain areas, class number 4 concerns arid and semi-arid areas, while classes 11 to 14 concern tropical forests. Fig. 3 shows the result of this procedure. Because classifications relying on both vegetation and thermal patterns are not widely available, a comparison has been made with a map of humidity patterns, realized by the CAZALAC (Centro del Agua para Zonas Áridas y semiáridas de Latino-América y el Caribe) center of Chile (Lobo et al., 2005). The choice of this classification as a comparison reference is due to the strong correlation between humidity regimes with both vegetation and thermal patterns. This classification is presented Fig. 4, and a correspondence between both classifications can be found in Table 1. In spite of various differences due to classifications nature, both classifications are similar in areas determination, the boundaries differing due to the low resolution of Reanalysis data. A comparison with GLCC (Global Land Cover Characteristics) classification built by the USGS (United States Geological Survey) has been also carried out, and the correspondence between both classifications' classes numbers can be found in Table 2, and a description of GLCC classes in Table 3. The GLCC classification can be downloaded from USGS website: http://edcsns17.cr.usgs.gov/glcc/. Because of the reduced number of classes of our final classification, in comparison with the 20 classes of the GLCC classification, the classes presented in this work correspond to more than one GLCC class, but the correspondence is coherent: the classes with low NDVI average (3) include

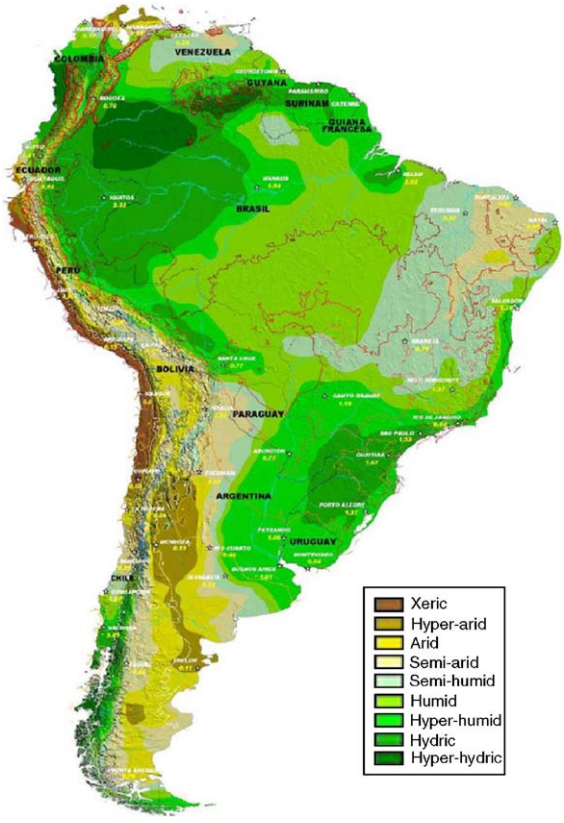

Fig. 4. Map of arid zones adapted from CAZALAC project. See text for details.

semi-arid vegetation (2, 8, 9, 19), while classes with high NDVI average values (7, 8, 9) include forests (13, 15) and green low vegetation (6, 7). The division of some GLCC classes in more than one of our classes is principally due to differences in thermal regimes.

4. Evolution

From the obtained classification, the evolution of vegetation can be studied during any period of time. First the yearly evolution will be studied, and then the long-term evolution over the 20 years of PAL data. This study is realized averaging, for each image, the values of a given parameter within a given class.

4.1. Yearly evolution

To study the evolution of the vegetation in South America on a yearly base, an average year was calculated month-by-month, for each estimated parameter. These average years of data were calculated as explained above in the case of NDVI. Yearly evolutions of LST and NDVI are shown respectively in Fig. 5a and b. To ensure that these evolutions were accurate, yearly evolution of air temperature at 2 m and precipitation are shown respectively (Fig. 5c and d). The two latter evolutions were elaborated from data obtained from the Reanalysis meteorological database.

Comparing Fig. 5a and c, one can observe that the evolutions have a similar pattern, with generally smaller thermal amplitude for Air Temperature. It can also be observed that the difference between both temperatures vary with classes, the classes representing denser vegetation being the ones with smaller temperature difference.

Fig. 5b and d also show similar evolution types, but with greater amplitude variations between classes.

Table 1
Description of the classes obtained from NDVI and thermal crossed classification in reference to Zapalac classification

Class number	Thermal pattern	Vegetation pattern	Description (according to Zapalac classes)
1	1	3	Arid (semi-arid)
2	1	6	Arid (semi-arid)+austral humid to hyper hydric regimes
3	2	3	Hyper arid, arid
4	3	3	Xeric, hyper arid
5	3	6	Semi-arid, sub humid
6	3	7	Humid, hydric
7	3	8	Hydric
8	4	6	Sub-humid Eastern Brazil
9	4	7	Humid, super humid
10	4	8	Hydric, hyper humid
11	5	6	Arid, semi-arid
12	5	9	Humid (hyper humid, hydric)
13	5	8	Hydric (hyper humid, humid)
14	5	7	Hyper hydric (humid)

See text for further description of vegetation and thermal patterns.

Table 2
Description of the classes obtained from PAL and Reanalysis crossed classification in reference to GLCC classification

Class number	Thermal pattern	Vegetation pattern	Description (according to GLCC classes)
1	1	3	7 – 8 – 9 – 19 – 21
2	1	6	7 – 8 – 10 – 15
3	2	3	8 – 9 – 10
4	3	3	2 – 8 – 19
5	3	6	2 – 5 – 6 – 7
6	3	7	10 – 13
7	3	8	2 – 6 – 7 – 13
8	4	6	2 – 5 – 6 – 7 – 8 – 10 – 18 – 19
9	4	7	2 – 6 – 7 – 10 – 13
10	4	8	2 – 6 – 7 – 13
11	5	6	2 – 5 – 6 – 8 – 10 – 13
12	5	9	13
13	5	8	13
14	5	7	13

See text for further description of vegetation and thermal patterns. See Table 3 for a description of GLCC classes.

Table 3
Description of GLCC classes

Class number	Description
1	Urban and built-up land
2	Dryland cropland and pasture
3	Irrigated cropland and pasture
4	Mixed dryland/irrigated cropland and pasture
5	Cropland/grassland mosaic
6	Cropland/woodland mosaic
7	Grassland
8	Shrubland
9	Mixed shrubland/grassland
10	Savanna
11	Deciduous broadleaf Forest
12	Deciduous needleleaf forest
13	Evergreen broadleaf forest
14	Evergreen needleleaf forest
15	Mixed forest
16	Water bodies
17	Herbaceous wetland
18	Wooded wetland
19	Barren or sparsely vegetated
20	Herbaceous tundra
21	Wooded tundra
22	Mixed tundra
23	Bare ground tundra
24	Snow or ice

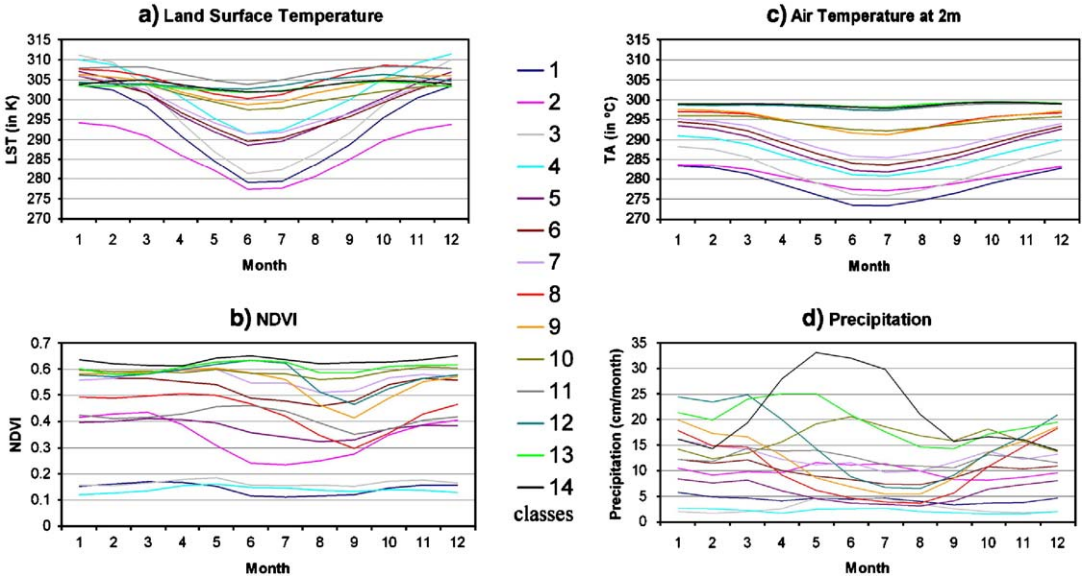

Fig. 5. Yearly evolutions (average of the 20-year data) of (a) Land Surface Temperature; (b) NDVI; (c) Air Temperature at 2 m height; (d) Precipitation. The first two data are obtained from PAL database, while the latter two are obtained from Reanalysis database.

Moreover, precipitation peaks can be observed for several classes, occurring in autumn or winter, generally followed by a NDVI peak, which can be easily explained by the fact that the limiting factor in vegetation growth is often the available quantity of water.

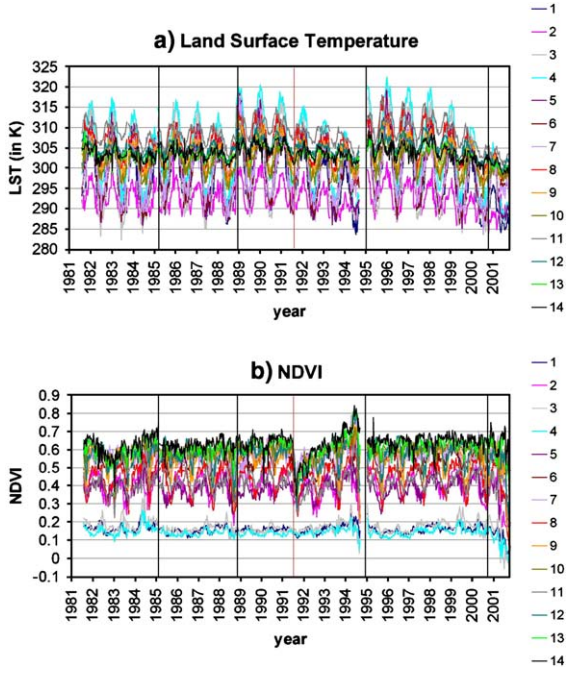

Fig. 6. Long-term evolutions of (a) Land Surface Temperature; (b) NDVI. The black vertical lines show satellite changes (see Table 1), while the red vertical line shows Mount Pinatubo's eruption (June 1991). (For interpretation of the references to color in this figure legend, the reader is referred to the web version of this article.)

4.2. Long-term evolution

Land Surface Temperature and NDVI long-term evolutions were computed for all the extent of the PAL database, ignoring composite periods for which one or more of the 5 bands were not available.

These results are shown Fig. 6a and b. On both graphs the dates of satellite changes (see Table 4) are shown as vertical black lines, and the eruption of Mount Pinatubo (June 1991) as a vertical red line.

Regarding long-term evolution of LST, it is obvious that satellite changes affect the data, and tend to make the temperature decrease during the activity period of each satellite, as has been demonstrated by Price (1991). This, due to orbital drift effect, needs therefore to be corrected, which will be next phase of the study (Jin and Treadon, 2003; Pinheiro et al., 2004).

Table 4
Satellite activity dates

Satellite number	Satellite activity dates
NOAA — 7	11/1981 – 01/1985
NOAA — 9	02/1985 – 10/1988
NOAA — 1	04/1989 – 09/1994
NOAA — 14	01/1995 – 07/2001
NOAA — 16	09/2000 →.....

Regarding NDVI long-term evolution, this effect cannot be observed, as was shown in Kaufmann et al. (2000). Nevertheless, it seems that Mount Pinatubo's eruption of June 1991 affect strongly the data, which can be explained by the large amount of aerosols emitted (Gleason et al., 2002).

Another effect can be observed at the end of the time period covered by the database: the NDVI seems to decrease independently of the class number, which could be explained by a technical problem with the AVHRR sensor on board of NOAA-16.

4.3. Discussion

Although the orbital drift effect on Land Surface Temperatures makes it impossible to study land cover evolution for the moment, the study detailed above proves the utility of our classification based on both thermal and vegetation patterns. The yearly evolutions shown above are in conformity with expected tendencies, as are the long-term evolutions, which confirm the homogeneity (in terms of NDVI and Land Surface Temperature values) of the defined classes.

5. Conclusions

In this paper have first been presented the algorithms used to determine Land Surface Temperature over the study area.

In a second part a classification of South America has been elaborated, using both vegetation types and thermal patterns. This classification has been built from PAL (concerning vegetation) and Reanalysis (concerning thermal patterns) data. This classification has been compared with other classifications of land cover and humidity regimes.

In a third part, preliminary results, concerning NDVI and Land Surface Temperature evolutions, have been exposed. These results confirm that Land Surface Temperature estimated from PAL data needs to be corrected from satellites orbital drift, which will be carried on during next phase of the study. Results concerning yearly evolution have also been exposed, which show expected tendencies, corroborated with meteorological data.

Acknowledgements

The authors wish to thank the AECI (project A/229/03), the European Union EAGLE project (SST3-CT-2003-502057), and the Ministerio de Ciencia y Tecnología (project REN2001-3105/CLI) for their financial support. The also authors wish to thank the Distributed Active Archive Center (Code 902.2) at the Goddard Space Flight Center, Greenbelt, MD, 20771, for producing the data in their present form and distributing them. The original data products were produced under the NOAA/NASA Pathfinder program, by a processing team headed by Ms. Mary James of the Goddard Global Change Data Center; and the science algorithms were established by the AVHRR Land Science Working Group, chaired by Dr. John Townshend of the University of Maryland. Goddard's contributions to these activities were sponsored by NASA's Mission to Planet Earth program.

References

Gleason, A., Prince, S., Goetz, S., Small, J., 2002. Effects of orbital drift on land surface temperature measured by AVHRR thermal sensors. Remote Sensing of Environment 79, 147–165.

Jin, M., Treadon, R.E., 2003. Correcting the orbit drift on AVHRR land surface skin temperature measurements. International Journal of Remote Sensing 24 (22), 4543–4558.

Kaufmann, R., Zhou, L., Knyazikhin, Y., Shabanov, N., Myneni, R., Tucker, C., 2000. Effect of orbital drift and sensor changes on the time series of AVHRR vegetation index data. IEEE Transactions on Geoscience and Remote Sensing 38 (6), 2584–2597.

Kistler, R., Kalnay, E., Collins, W., Saha, S., White, G., Woollen, J., Chelliah, M., Ebisuzaki, W., Kanamitsu, M., Kousky, V., van den Dool, H., Jenne, R., Fiorino, M., 2001. The NCEP-NCAR 50-year reanalysis: monthly means CD-ROM and documentation. Bulletin of the American Meteorological Society 82, 247–267.

Lobo, L.D., Gabriels, D., Ovalles, F.V., Santibañez, F., Moyano, M.C., Aguilera, R., Pizarro, R., Sangüesa, C., Urra, N., 2005. Guía metodológica para la elaboración del mapa de zonas áridas, semiáridas y subhúmedas secas de América Latina y el Caribe. UNESCO-PHI Program. website: http://www.cazalac.org/mapa_alc_guia.html.

Morales, L., Castellaro, G., Sobrino, J.A., El Kharraz, J., 2004. Land cover dynamic monitoring in the region of Coquimbo (Chile) by the analysis of multitemporal NOAA-AVHRR NDVI images. ISPRS Conference, Commission VI, 12–23 July 2004, Istanbul, Turquia.

Nemani, R., Running, S., 1997. Land cover characterization using multitemporal Red, Near-IR, and thermal-IR data from NOAA/AVHRR. Ecological Applications 7 (1), 79–90.

Pinheiro, A., Privette, J., Mahoney, R., Tucker, C., 2004. Directional effects in a daily AVHRR land surface temperature dataset over Africa. IEEE Transactions on Geoscience and Remote Sensing 42 (9), 1941–1954.

Price, J.C., 1991. Timing of NOAA afternoon passes. International Journal of Remote Sensing 12, 193–198.

Réaumur, R.A.F. de, 1735. Observations du thermomètre. Acad. Roy. des xi. des Pays-Bas Mem. pp. 737–754.

Saunders, R.W., Kriebel, K.T., 1988. An improved method for detecting clear sky and cloudy radiances from AVHRR data. International Journal of Remote Sensing 9, 123–150.

Sobrino, J.A., Raissouni, N., 2000. Toward remote sensing methods for land cover dynamic monitoring: application to Marocco. International Journal of Remote Sensing 21, 353–363.

Sobrino, J.A., Raissouni, N., Simarro, J., Nerry, F., Petitcolin, F., 1999. Atmospheric water vapor content over land surfaces derived from the AVHRR data: application to the Iberian Peninsula. IEEE Transactions on Geoscience and Remote Sensing 37, 1425–1434.

Thornthwaite, C.W., 1948. An approach toward a rational classification of climate. Geographical Review 38, 55–94.

Ulivieri, C., Castronuovo, M.M., Francioni, R., Cardillo, A., 1994. A split window algorithm for estimating land surface temperature from satellites. Advances in Space Research 14 (13), 59–65.